Journal of Materials Chemistry C

Accepted Manuscript

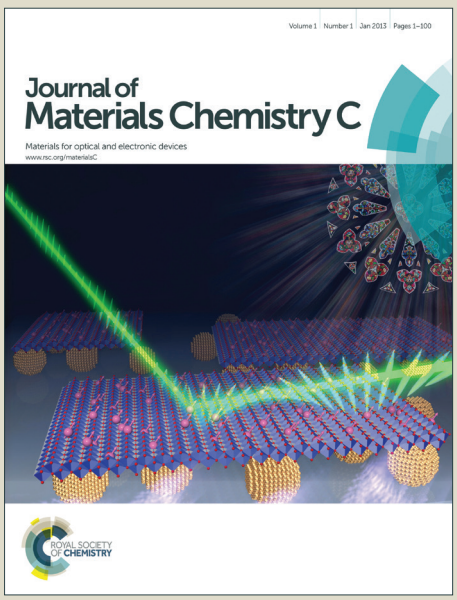

ROYAL SOCIETY OF CHEMISTRY

www.rsc.org/materialsC

Journal Name

RSCPublishing

ARTICLE

β-Iminoenolate Boron Complex with Terminal Triphenylamine Exhibiting Polymorphism and Mechanofluorochromism

Cite this: DOI: 10.1039/x0xx00000x

Received 00th January 2012,
Accepted 00th January 2012

DOI: 10.1039/x0xx00000x

www.rsc.org/

Zhenqi Zhang,[a] Zhu Wu,[a] Jingbo Sun,[a] Boqi Yao,[a] Pengchong Xue[a] and Ran Lu*[a]

New β-iminoenolate boron complex with terminal triphenylamine (**TP**) was synthesized, and it could emit strong fluorescence in solutions and in solid states. Two kinds of crystals were gained via evaporation the solutions of **TP** in different solvents. Yellow ribbon-liked crystal (Y-crystal) giving yellowish green emission centered at 518 nm was obtained from tetrahydrofuran (THF) solution, and green needle-like crystal (G-crystal) emitting green light with maximum emission at 495 nm was yielded from dichloromethane (DCM)/petroleum ether solution. It was found that the molecules adopted a stacking mode of *J*-aggregation in Y-crystal, and the π-π interaction in G-crystal was weaker than that in Y-crystal. Besides the polymorphism feature, **TP** exhibited mechanofluorochromic (MFC) properties. Upon ground, the Y-crystal and G-crystal could transform into similar ground powders with yellow emission centered at 533 nm. Interestingly, when the ground powder formed from Y-crystal or G-crystal was fumed with DCM or heated, the XRD pattern and the fluorescence emission spectrum of the fumed sample would be recovered to their own initial crystal states. Such memory ability of the molecular packing mode during reversible MFC processes might be useful for our well understanding MFC mechanism.

Introduction

Organic solid-state luminescent materials have been widely studied over the past decade because of their excellent optoelectronic properties and applications in organic light-emitting diodes (OLED),[1] organic semiconductors,[2] organic solid-state lasers[3] and organic fluorescent sensors.[4] The traditional way to obtain different luminescent materials was developing new π-conjugated skeletons or modifying the known skeletons with different functional groups. On the other side, it was found that the solid-state luminescent properties did not only depend on the molecular structures but also depended on the molecular packing modes in the crystals. The conformational- and packing-dependent polymorphs was first defined by McCrone in 1965, "A polymorph is a solid crystalline phase of a given compound resulting from the possibility of at least two different arrangements of the molecules of that compound in the solid state."[5] Recently, many kinds of polymorphism materials have been developed.[6] For example, Wang *et al.* synthesized triphenylamine functionalized thiazole derivative giving four types of crystals with molecular-conformational and packing dependent luminescent properties.[7] On the other hand, mechanofluorochromic (MFC) materials, whose emitting colours changed in response to external mechanical forces (such as grinding, crushing, rubbing, etc.) because of the different molecular stacking modes in solid states, have attracted increasing attention and extended the application of solid-state luminescent materials.[8] For example, the derivatives of tetraphenylethene,[9] 9,10-divinylanthracene[10] and oligo(*p*-phenylene vinylene),[11] as well as β-diketone boron complexes have been found to show MFC activities.[12] However, the solid emitters exhibiting polymorphism and MFC properties were seldom reported.[13] Tang and coworkers found that the propeller-shaped diphenyldibenzofulvene derivative could form two kinds of single crystals, in which one emitted green light and other gave yellow emission. Interestingly, the two kinds of crystals could be transformed into non-emissive amorphous solids upon grinding and the emission could be recovered to their initial states after thermal treatment at different temperature.[14] Tian *et al.* obtained three kinds of single crystals of divinylanthracene derivative, and found that the green-emitting crystal could be transformed into the yellow-emitting and orange-emitting crystals under pressure.[15] The investigation of the changeable fluorescence induced by polymorphism and mechanical forces would help us to well understand MFC mechanism and to design multi-channels fluorescence response

materials. In our previous work, we have found that D-π-A type β-iminoenolate boron complexes with non-planar conjugated moieties exhibited high-contrast MFC properties.[16] With a propeller-like conformation, triphenylamine is an electron donor and a building block in functional organic materials applied in OLED,[17] organic photovoltaic cells,[18] nonlinear optical materials,[19] fluorescent sensors[20] , aggregation-induce emission[21] and MFC materials.[22] We also found that triphenylamine unit could tune the strength of π-π interaction and helped molecules to self-assemble into 1D nanofibers.[23] With these in mind, herein, we design a new D-π-A type β-iminoenolate boron complex with terminal triphenylamine **TP** (Scheme 1). It was interesting that the green needle-like crystal (G-crystal) emitting green fluorescence and the yellow crystal (Y-crystal) emitting yellowish-green light could be gained via slow evaporation of its DCM/petroleum ether and THF solutions, respectively. It was found that the molecules packed into *J*-aggregates in Y-crystal and the π-π interaction between **TP** molecules was weaker in G-crystal than that in Y-crystal. When either G-crystal or Y-crystal was ground, the ground powders emitting yellow fluorescence were yielded. After the ground powders were fumed by DCM or heated, the emission could be recovered only to their own initial states. The memory of the molecular packing modes of **TP** during MFC processes might be useful for our well understanding MFC mechanism and designing new MFC materials.

Experimental Section

Measurement and characterization. ^{1}H NMR spectra was measured with a Mercury Plus instrument at 400 MHz by using DMSO-d_6 as solvent. ^{13}C NMR spectra was measured with a Mercury Plus instrument at 100 MHz by using DMSO-d_6 as solvent. FT-IR spectrum was measured with a Nicolet-360 FT-IR spectrometer by incorporation of sample in KBr disk. The UV-vis absorption spectra were obtained on Shimadzu UV-3100 spectrophotometer. Fluorescent emission spectra were obtained on a Cary Eclipse fluorescence spectrophotometer. Mass spectra were obtained with Agilent 1100 MS series and AXIMA CFR MALDI-TOF (Compact) mass spectrometers. C, H, and N elemental analyses were performed with a Perkin-Elmer 240C elemental analyzer. XRD patterns were obtained on an Empyrean X-ray diffraction instrument. Single crystal of **TP** was selected for X-ray diffraction studies in a Rigaku RAXIS-RAPID diffractometer. Cyclic voltammograms were obtained on a CHI 604C voltammetric analyzer with a scan rate at 50 mV/s. A three electrode configuration was used for the measurement: a platinum button as the working electrode, a platinum wire as the counter electrode, and a saturated calomel electrode (SCE) as the reference electrode. The solution of $(C_4H_9)_4NBF_4$ in CH_2Cl_2 (0.1 M) was used as the supporting electrolyte. The ground powders were prepared by grinding Y-crystal or G-crystal with a pestle in the mortar. The heated samples were obtained by heating the ground powders at 100 °C for 5 s. The fumed samples were obtained by fuming the ground powders with DCM vapor for 5 s. The high-temperature annealed samples were obtained via the following process: the samples were heated from 20 °C to 230 °C (above their melting points) at heating rate of 10 °C/min. After the isothermal process was lasted for 2 min, the samples were cooled from 230 °C to 20 °C at cooling rate of 10 °C/min.

Synthesis. THF was dried over sodium and diphenyl ketone. CH_2Cl_2 was dried over calcium hydride. The other chemicals and reagents were used as received without further purification.

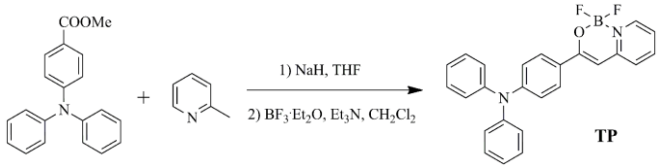

Scheme 1. Synthetic route for **TP**.

3-(4-(diphenylamino)phenyl)-1,1-difluoro-1H-pyrido[1,2-c][1,3,2]oxazaborinin-9-ium-1-uide (TP): NaH (60 %, 0.60 g, 15.14 mmol) was added to a solution of 2-methylpyridine (1.10 mL, 12.62 mmol) in THF (50mL) at 0 °C. Then, methyl 4-(diphenylamino)benzoate (1.90 g, 6.31 mmol) was added and the mixture was stirred at room temperature for 30 min. After the mixture was refluxed under an atmosphere of nitrogen for 24 h, it was cooled to room temperature. After that, the mixture was acidified with dilute HCl and a yellow solid was collected by suction filtration. The solid was dried under vacuum followed by dissolved in CH_2Cl_2 (50 mL). Boron trifluoride diethyl ether complex (4.00 mL, 31.55 mmol) and triethylamine (4.40 mL, 31.55 mmol) were added to the above solution, which was stirred at room temperature for 24 h. Water was added (200 mL) in order to quench the reaction. The organic layer was separated and dried over Na_2SO_4. After removal of the solvent, the crude product was purified by column chromatography (silica gel, DCM/ petroleum ether, v/v = 3/1) to afford **TP** (0.55 g) as a yellow solid. Yield 42%; m.p. 184.0-186.0 °C; ^{1}H NMR (400 MHz, DMSO-d_6) δ 8.44 (d, J = 4.0 Hz, 1H), 8.16 (m, 1H), 7.81 (m, 2H), 7.59 (d, J = 8.0 Hz, 1H), 7.48 (m, 1H), 7.38 (m, 4H), 7.14 (m, 6H), 6.97 (d, J = 8.0 Hz, 2H), 6.74 (s, 1H). ^{13}C NMR (100 MHz, DMSO- d_6) δ 160.35, 150.87, 149.76, 146.31, 142.48, 139.50, 129.78, 127.39, 126.18, 125.27, 124.33, 122.73, 120.97, 120.47. FT-IR (KBr, cm^{-1}): 700, 758, 766, 808, 910, 916, 1022, 1072, 1099, 1125, 1147, 1169, 1193, 1216, 1269, 1303, 1324, 1335, 1489, 1502, 1536, 1589, 1605, 1629, 2851, 2923; MALDI-TOF MS: m/z: calculated for $C_{25}H_{19}BF_2N_2O$: 412.2; found: 413.2 $[M+H]^+$. Elemental analysis (%): C 72.84, H 4.65, N 6.80; found: C 72.98, H 4.69, N 6.84.

Results and discussion

Synthesis

The synthetic route for β-iminoenolate boron complex **TP** was shown in Scheme 1. Firstly, methyl 4-(diphenylamino)benzoate was synthesized according to the reported procedures.[24] Then,

the condensation coupling reaction between 2-methylpyridine and 4-(diphenylamino)benzoate afforded the corresponding β-iminoenolate intermediates, which was complexed with boron trifluoride diethyl ether directly without further purification to yield β-iminoenolate boron complex **TP**. The target molecule was characterized by ^{1}H NMR, ^{13}C NMR, MALDI-TOF mass spectrometry, FT-IR and C, H, N elemental analyses (see Supporting Information). It was found that the synthesized β-iminoenolate boron complex was well dissolved in CH_2Cl_2, THF, ethanol, and so on.

UV-vis absorption and fluorescence emission spectra in solutions

The UV-vis absorption and fluorescence emission spectra of **TP** in different solvents were shown in Figure 1, and the corresponding photophysical data were summarized in Table S1. It was clear that **TP** gave two obvious absorption bands at ca. 300 nm and ca. 420 nm in the solvents, and the latter one was derived from intramolecular charge transfer (ICT) transition, which could be confirmed by the solvent-dependent emission spectra. In the case of maximum absorption, in nonpolar solvent of cyclohexane **TP** exhibited vibrational structure with two peaks (419 nm and 437 nm), which disappeared in polar solvents due to the interaction between **TP** and solvent molecules. As shown in Figure 1b and S1, we found that **TP** emitted blue light in cyclohexane, and the emission gave vibrational structure. The fluorescence emission bands of **TP** appeared at 453 nm and 479 nm in cyclohexane. With increasing the solvent polarities, the emission band of **TP** red-shifted significantly. For example, it emitted yellow light centered at 547 nm in DMSO. We found that the Stokes shift increased from 1791 to 5700 cm^{-1} with increasing the solvent polarity. Meanwhile, the maximum emission energy showed a linear relationship with the solvent polarity $E_T(30)$ (Figure S2). Moreover, the fluorescence quantum yields decreased from 0.77 in cyclohexane to 0.38 in DMSO using 9,10-diphenylanthracene in benzene (Φ_F = 0.85) as standard. Therefore, the significant red-shift of emission band, the large Stokes shifts and the decreased fluorescence quantum yields in polar solvents compared with those in non-polar solvents, and a linear relationship between the maximum emission energy and solvent polarity suggested that the emission was derived from ICT transition.[25]

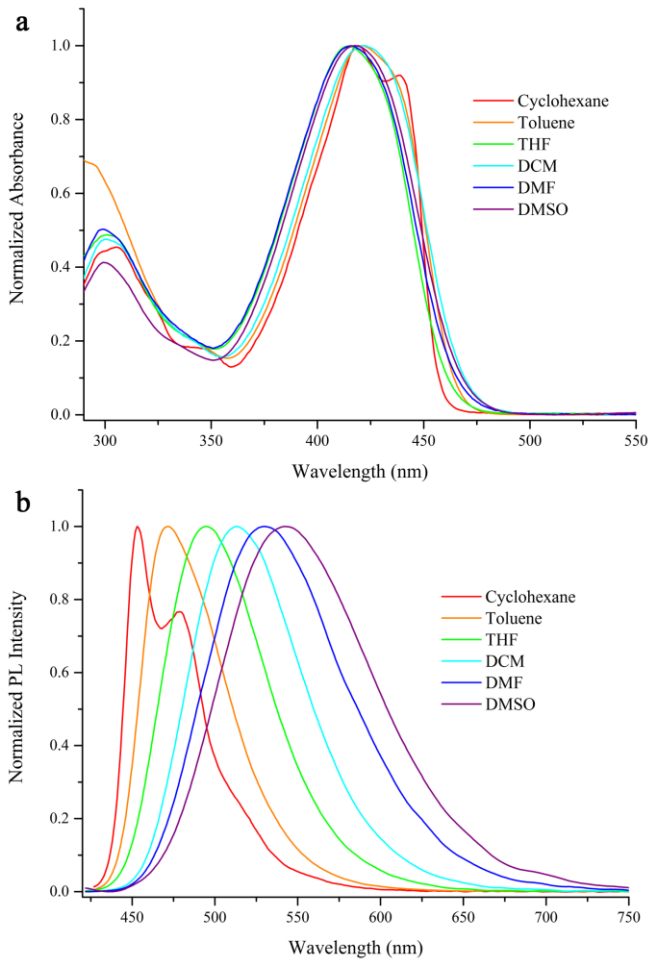

Figure 1. UV-vis absorption and fluorescence emission (λ_{ex} = 415 nm) spectra of **TP** in different solvents (1.0 x 10^{-5} mol/L).

Electrochemical property

To obtain the HOMO and LUMO energy levels, the electrochemistry property of **TP** was studied and the cycle voltammogram was shown in Figure S3. **TP** exhibited one reversible reduction process and the half-wave potential was located at −2.26 V (*vs* Fc/Fc$^+$). The HOMO and LUMO energy levels were calculated using the empirical equations: $E_{LUMO} = -(E_{red} + 4.8)$ and $E_{HOMO} = E_{LUMO} - E_g$, in which E_g was estimated from the onset of the absorption spectrum ($E_g = 1240 / \lambda_{onset}$). As a result, the HOMO and LUMO energy levels were determined to be -5.19 eV and -2.54 eV, respectively (table 1).

Table 1. HOMO and LUMO energy levels of **TP**.

E^{red} (V)[a]	LUMO (eV)[b]	HOMO (eV)[b]	E_g (eV)[c]	HOMO (eV)[d]	LUMO (eV)[d]
-2.26	-2.54	-5.19	2.65	-2.08	-5.16

[a] E^{red}=; potencials versus Fc/Fc$^+$, working electrode platinum button, 0.1M $(C_4H_9)_4NBF_4$-DCM, scan rate 50mV/s, Fc/Fc$^+$ was used as external reference. [b] Calculated using the empirical equation: E_{LUMO}= -(E^{red}+4.8) and E_{HOMO} = E_{LUMO}+E_g.[c] Estimated from the onset of the absorption spectrum (E_g=1240/λ_{onset}).[d] Obtained from quantum chemical calculation using DFT/B3LYP/6-31G.

Theoretical calculation

To well understand the electronic structure of **TP**, the density functional theory (DFT) calculation was carried out by Gaussian 09W program using DFT/B3LYP/6-31G method.[26] The frontier orbital plots of HOMO and LUMO were shown in Figure 2. The HOMO was mainly distributed in the electron donor of triphenylamine unit and the LUMO was concentrated on the electron acceptor of β-iminoenolate boron moiety. The separated HOMO and LUMO indicated that ICT could occur.

Meanwhile, the HOMO and LUMO energy levels were also obtained by theoretical calculation. As shown in Table 1, the HOMO and LUMO energy levels were located at -2.08 and -5.16 eV. The calculated LUMO energy level was close to the result from electrochemical measurement.

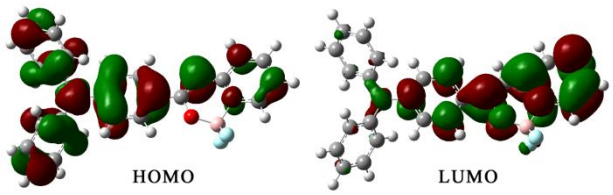

Figure 2. The frontier orbital plots of the HOMO and LUMO of **TP**.

Polymorphism properties

Two kinds of crystals have been obtained via slow evaporation of **TP** in different solvents. The yellow ribbon-like crystal (Y-crystal) was gained from THF solution and the green needle-like crystal (G-crystal) was obtained from DCM/petroleum ether solution. The fluorescence emission spectra of the two kinds of crystals were shown in Figure 3. It was clear that Y-crystal emitted yellowish green fluorescence centered at 518 nm and the maximal emission peak of G-crystal was located at 495 nm. Compared with the emission in toluene, the emission peaks of **TP** in Y-crystal and G-crystal gave red-shift of 45 nm and 22 nm, respectively, which might be attributed to π-π interactions in the solid states. Meanwhile, the UV-vis spectra of **TP** in Y-crystal and G-crystal were measured in a reflection way and the spectra were shown in Figure 3. We found that the maximum absorption bands of Y-crystal and G-crystal emerged at ca. 450 nm and ca. 440 nm, respectively, giving red-shift of ca. 30 nm and 20 nm, respectively, relative to that in toluene. It suggested that π-π interaction happened in crystals. It should be noted that the absorption and emission bands of Y-crystal appeared in low energy region compared with those of G-crystal. We deduced that the **TP** molecules packed more closely in Y-crystal and the π-π interaction was stronger in Y-crystal than that in G-crystal.

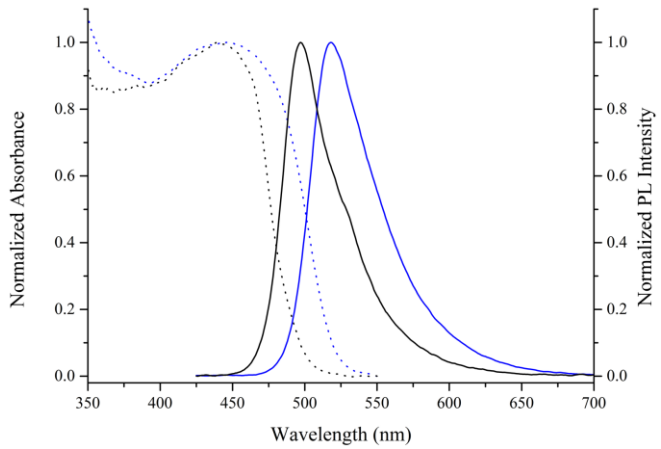

Figure 3. UV-vis (dot line) and fluorescence emission (solid line, λ_{ex} = 415 nm) spectra of **TP** in Y-crystal (black) and G-crystal (blue).

To better understand the relationship between the photophysical properties and molecular packing modes of **TP** in different crystals, the crystal structure of Y-crystal was measured by single-crystal X-ray diffraction and shown in Figure 4. As shown in Figure 4a, **TP** had a nonplanar configuration, and the boron atom stuck up out of the pyridine ring. The dihedral angle between the pyridine and the benzene rings was 16.52 °.

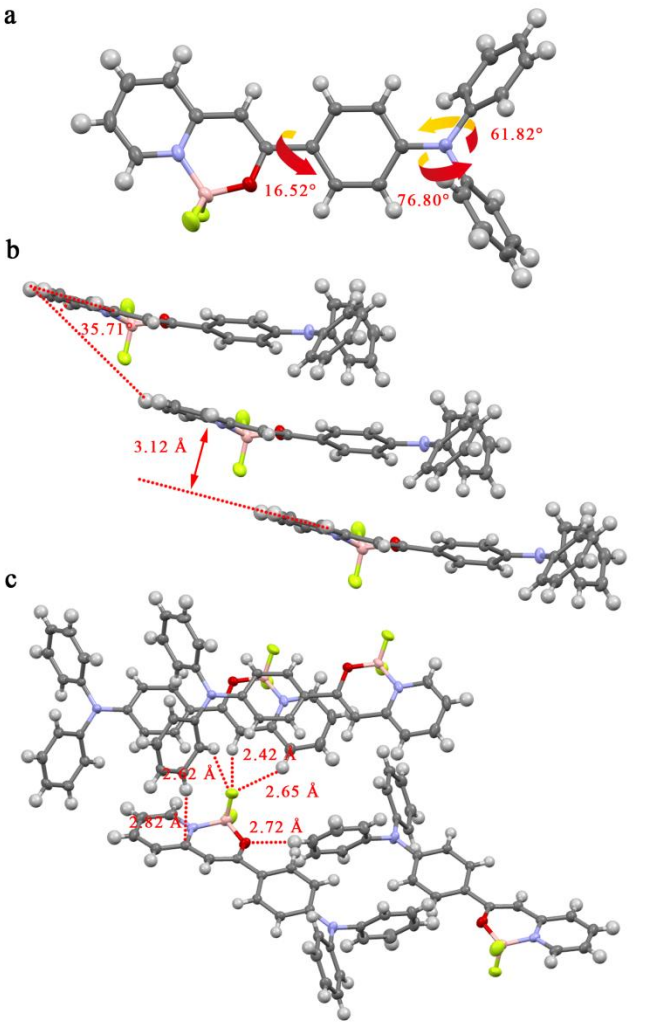

Figure 4. Molecular configuration (a), stacking mode (b) and intermolecular interactions (c) of **TP** in Y-crystal.

The dihedral angles between three benzene rings of triphenylamine were 61.82 ° and 76.80 °. The adjacent distance of the molecular planes was 3.12 Å and the sliding angle was 35.71 ° (Figure 4b). Therefore, *J*-aggregates were formed in Y-crystal. Meanwhile, the hydrogen bonds of C-H ··F, C-H ··O and C(Ar)-H ··π were involved in the crystal. In particular, one fluorine atom in the central molecule formed three kinds of hydrogen bonds with the hydrogen atoms in pyridine ring, methylene on the boron ring and triphenylamine, and the

distances of the short contacts were 2.42 Å, 2.65 Å and 2.62 Å, respectively. Another fluorine atom was free from hydrogen bond. Moreover, the distance for the hydrogen bond between oxygen and hydrogen atoms in the triphenylamine moiety was 2.72 Å. The distance of C(Ar)-H···π interaction between the hydrogen atom and the carbon atom in pyridine was 2.82 Å. Herein, the formation of *J*-aggregates in Y-crystal of **TP** could explain the red-shift of absorption and emission compared with those in toluene. Unfortunately, we could not gain the single crystal structure of G-crystal by single-crystal X-ray diffraction. However, low and wide angle powder X-ray diffraction patterns could provide useful information on the molecular packing. From Figure 5 we could find three diffraction peaks (2θ= 4.40 °, 8.81 ° and 13.28 °) and the corresponding *d*-spacing values were 20.05 Å, 10.02 Å and 6.66 Å, respectively, with a ratio of ca. 1:1/2:1/3. It indicated that the molecules adopted a lamellar stacking mode. The period of the stacking was 20.05 Å, which was longer than the length of the molecule, so we deemed that head-to-tail dimers might be involved in one layer. The possible molecular packing mode in G-crystal was proposed in Figure S4.

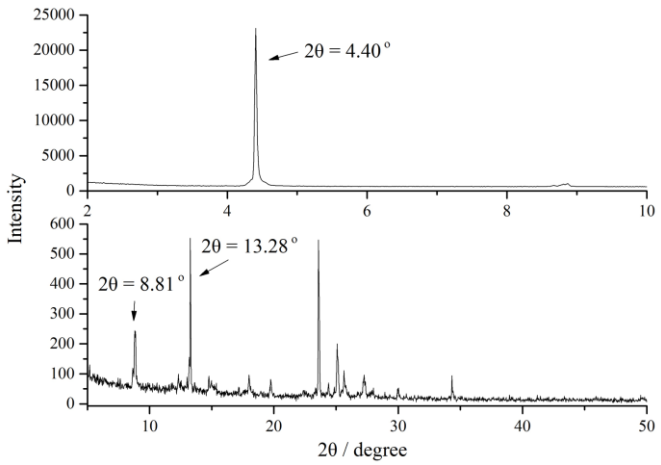

Figure 5. Low and wide angle XRD patterns of G-crystal of **TP**.

Mechanofluorochromic properties

In our previous work, we found the β-iminoenolate boron complexes with D-π-A structures exhibited MFC properties. Herein, we intended to investigate the MFC properties of Y-crystal and G-crystal of **TP**. As shown in Figure 6, we found that the Y-crystal emitting yellowish green fluorescence with a maximum at 518 nm could be changed into the powder emitting yellow light centered at 533 nm after ground. When the ground powder was fumed with DCM or heated at 100 ℃ for 5 s, the fluorescence was restored. This change of emitting colour was reversible under grinding and solvent fuming or thermal treatment (Figure S5). Interestingly, G-crystal exhibited a sharp fluorescence colour change. After ground, green G-crystal changed into yellow powder, and the emitting colour changed from green (495 nm) to yellow (533 nm). The ground powder could also be transformed to the initial green solid with emission at 495 nm after fumed by DCM or heated at 100 °C for 5 s. This process was also reversible (Figure S6). Interestingly, although the ground powders, which were obtained from Y-crystal and G-crystal via grinding, exhibited same emission spectra, the emission could only recover to the original state after fumed with DCM. We also tested the response of the ground powders to different solvent fuming, and found that the emitting colour of the fumed samples did not depend on the kinds of solvents but on the initial crystal states. For example, after the ground powder obtained from G-crystal was fumed with DCM or THF, the emission of the fumed sample was similar to that of G-crystal instead of Y-crystal although Y-crystal was gained from its THF solution.

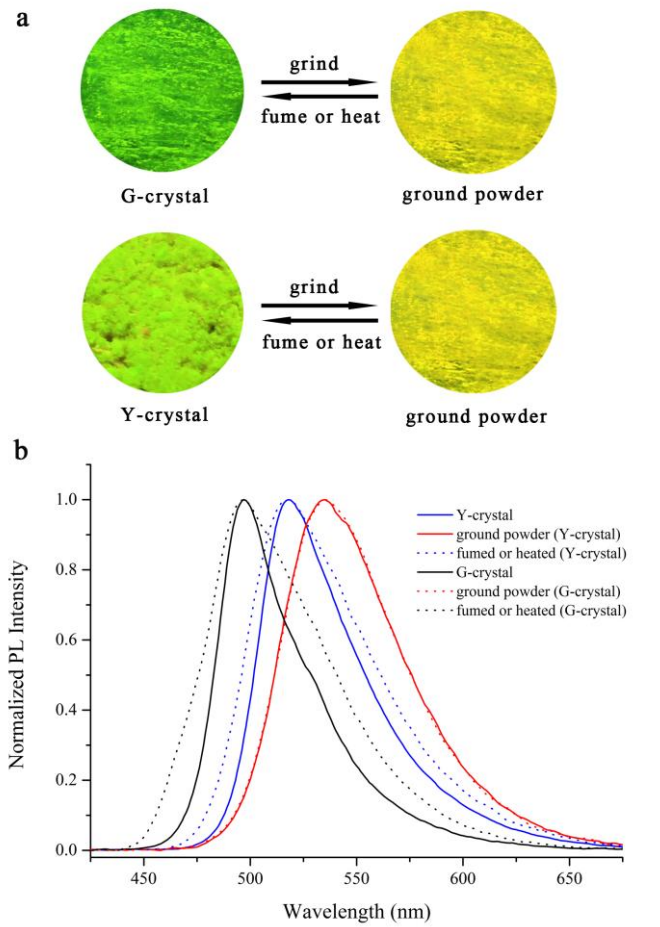

Figure 6. (a) Photos of solid **TP** under UV light and (b) fluorescence emission spectra of **TP** in different solid states (λ_{ex} = 415 nm).

To explain MFC mechanism, XRD patterns and UV-vis spectra of **TP** in different solid states were measured. Figure 7 illustrated that Y-crystal exhibited several strong and evident diffraction peaks due to its well-ordered crystalline structure. After Y-crystal was ground, no obvious diffraction peak was detected, indicating that the ordered crystalline structure was destroyed and the ground powder was in amorphous state. Meanwhile, after DCM fuming or heated, the diffraction peaks recovered because of the transformation from amorphous to

crystalline state again. G-crystal also exhibited strong diffraction peaks, which were different from those for Y-crystal because of the different molecular packing mode. Similarly, the ground powder obtained from G-crystal gave no diffraction peak due to its amorphous phase. When the ground powder formed from G-crystal was fumed with DCM or heated, most of the diffraction peaks recovered. Remarkably, the ground powders obtained from Y-crystal or G-crystal recovered to their initial crystal states after solvent fuming, respectively. Moreover, UV-vis spectra of **TP** in different solid states were

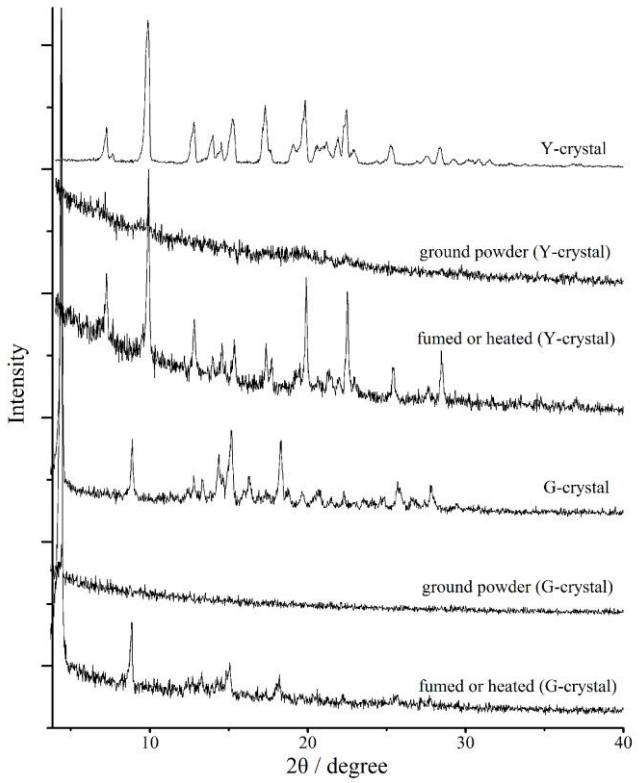

Figure 7. XRD patterns of **TP** in different solid states.

measured in a reflection way and shown in Figure S7. Y-crystal gave a maximum absorption at ca. 450 nm. After it was ground, the absorption peak red-shifted to 470 nm. When the ground powder was fumed with DCM or heated, the absorption band recovered back to 450 nm. G-crystal showed a maximum absorption band at 440 nm and the absorption of the corresponding ground powder was located at 470 nm. After fumimg or heating, it turned back to 440 nm. Combining with the XRD patterns, emission and absorption spectra of **TP** in different solid states, we proposed the MFC mechanism as below. After Y-crystal was ground, the ordered crystalline structure was changed into disordered amorphous state. The distance between molecules became shorter and the intermolecular interaction was stronger, so the absorption band and emission band red-shifted. When the ground powder was fumed or heated, the amorphous state recovered back to the crystalline structure, as a result, the emission was recovered. G-crystal underwent the similar processes. Although the crystalline states could be damaged after grinding Y-crystal and G-crystal, molecular stacking mode could not be destroyed totally. In other words, the molecular packing mode might be memorized to some extent. Thus, when the ground powders were fumed or heated, the molecular packing mode and the emission could be recovered to their initial crystal states. However, such interesting memory ability was damaged when the ground powders obtained from Y-crystal and G-crystal were heated above the melting point, and the corresponding samples were named as high-temperature annealed samples. Figure S8 showed the DSC curves of Y-crystal and the ground powder obtained from Y-crystal. In the heating process Y-crystal gave an evident endothermic peak at 187.0 °C, corresponding to its melting point. Except the endothermic peak at 186.0 °C, another peak at 85.0 °C emerged in the heating process of the ground powder, indicating the transition from amorphous to crystalline states. However, in the cooling process no crystallization peak was observed. It meant that the high-temperature annealed sample of Y-crystal or its ground powder was in amorphous state, which was quite different from the recovery of crystalline state of the heated sample obtained by heating the ground powder at 100 °C. It illustrated the disappearance of the memory of the molecular packing mode if the ground powder was annealed at temperature over the melting point. Similar DSC curves were observed for G-crystal and its ground powder (Figure S9), and the melting point of G-crystal was found to be 186.0 °C. Therefore, the different molecular stacking mode has less effect on the melting point. On the other hand, no evident diffraction peaks could be detected in XRD patterns of the high-temperature annealed sample of Y-crystal, G-crystal or their ground powders (Figure S10), meaning amorphous state. Thus, it was understandable that the emission of the high-temperature annealed sample of Y-crystal, G-crystal or their ground powders was located at 535 nm (Figure S11), which was similar to that of the ground powders. We deduced that the memory ability of the molecular packing mode in ground powder could be destroyed upon heated over the melting point due to the total break of intermolecular interactions, but the original crystalline state could be recovered when some weak intermolecular interactions were still maintained in amorphous ground powder.

Conclusions

In summary, we have synthesized a new β-iminoenolate boron complex with terminal triphenylamine, which exhibited strong fluorescence emission in solutions and in solid states. Through slow evaporation of the THF and DCM/petroleum ether solutions of **TP**, yellow ribbon-liked crystal (Y-crystal) and green needle-like crystal (G-crystal) were obtained, respectively. The Y-crystal gave yellowish green emission with a maximum emission peak at 518 nm and G-crystal emitted green light (495 nm). Since the absorption and emission bands of Y-crystal appeared in long wavelength region compared with those for G-crystal, we deduced that the π-π interaction in Y-crystal was stronger than that in G-crystal. When the two kinds of crystals

were ground, the formed ground powders in amorphous states emitted same yellow fluorescence centered at 533 nm. However, after the ground powders were fumed or heated, the XRD patterns and the emission spectra could only be converted back to their initial crystal states. Such memory ability of the molecular packing mode might be useful for our well understanding of MFC mechanism.

Acknowledgements

This work is financially supported by the National Natural Science Foundation of China (21374041), the Open Project of State Key Laboratory of Supramolecular Structure and Materials (SKLSSM2015014).

Notes and references

[a] State Key Laboratory of Supramolecular Structure and Materials, College of Chemistry, Jilin University, Changchun, P. R. China. E-mail: luran@mail.jlu.edu.cn

† Electronic Supplementary Information (ESI) available: [^{1}H NMR, ^{13}C NMR, MALDI/TOF MS and CV spectra; photos of **TP** in different solvents under UV light; UV-vis spectra in different solid states; reversibility of MFC processes; DSC curves, XRD patterns and PL spectra of the high-temperature annealed samples]. CCDC 1410444 for **TP**. For ESI and crystallographic data in CIF see DOI: 10.1039/b000000x/

1 a) A. C. Grimsdale, K. L. Chan, R. E. Martin, P. G. Jokisz, A. B. Holmes, *Chem. Rev*., 2009, **109**, 897-1091; b) S. M. Kelly, *Flat Panel Displays: Advanced Organic Materials*, ed. J. A. Connor, The Royal Society of Chemistry, Cambridge, 2000; c) C. W. Tang and S. A. Van Slyke, *Appl. Phys. Lett*., 1987, **51**, 913-915; d) R. H. Friend, R. W. Gymer, A. B. Holmes, J. H. Burroughes and R. N. Marks, *Nature*, 1999, 397, 121-128; e) J. H. Lee, Y. Y. Yuan, Y. J. Kang, W. L. Jia, Z. H. Lu and S. N. Wang, *Adv. Funct. Mater*., 2006, **16**, 681-686; f) P. L. Burn, S.-C. Lo and I. D. W. Samuel, *Adv. Mater*., 2007, **19**, 1675-1688.

2 a) A. P. Kulkarni , C. J. Tonzola , A. Babel and S. A. Jenekhe, *Chem. Mater*., 2004, **16**, 4556-4573; b) K. Nomura, H. Ohta, A. Takagi, T. Kamiya, M. Hirano and H. Hosono, *Nature*, 2004, **432**, 488-492; c) A. R. Murphy and J. M. J. Fréchet, *Chem. Rev*., 2007, **107**, 1066-1096; d) V. Coropceanu, J. Cornil, D. A. da Silva Filho, Y. Olivier, R. Silbey and J.-L. Brédas, *Chem. Rev*., 2007, **107**, 926-952; e) L.-L. Chua, J. Zaumseil, J.-F. Chang, Eric C.-W. Ou, P. K.-H. Ho, H. Sirringhaus and R. H. Friend, *Nature*, 2005, **434**, 194-199.

3 a) I. D. W. Samuel, G. A. Turnbull, *Chem. Rev*. 2007, **107**, 1272-1295; b) U. Scherf, S. Riechel, U. Lemmer, R. F. Mahrt, *Curr. Opin. Solid State Mater. Sci*., 2001, **5**, 143-154; c) M. D. McGehee, A. J. Heeger, *Adv. Mater*., 2000, **12**, 1655; d) G. Kranzelbinder, G. Leising, *Rep. Prog. Phys*., 2000, **63**, 729-762; e) N. Tessler, *Adv. Mater*., 1999, **11**, 363-370; f) V. G. Kozlov, S. R. Forrest, *Curr. Opin. Solid State Mater. Sci*., 1999, **4**, 203-208.

4 a) J. S. Yang, T. M. Swager, *J. Am. Chem. Soc*., 1998, **120**, 11864-11873; b) J. S. Yang, T. M. Swager, *J. Am. Chem. Soc*., 1998, **120**, 5321-5322; c) L. Zang, Y. Che and J. S. Moore, *Acc. Chem. Res*., 2008, **41**, 1596-1608; d) Z. Ning, Z. Chen, Q. Zhang, Y. Yan, S. Qian, Y. Cao and H. Tian, *Adv. Funct. Mater*., 2007, **17**, 3799-3807. e) T. J. Dale, J. Rebek, *J. Am. Chem. Soc*., 2006, **128**, 4500-4501; f) S. W. Zhang, T. M. Swager, *J. Am. Chem. Soc*., 2003, **125**, 3420-3421.

5 W. McCrone, Physics and chemistry of the organic solid state, Chapter 8, pp. 725–767, vol. 2, Polymorphism, Interscience, New York, 1965.

6 a) J.-P. Brog, C.-L. Chanez, A. Crochet and K. M. Fromm, *RSC Adv*., 2013, **3**, 16905-16931; b) D. Yan and D. G. Evans, *Mater. Horiz*., 2014, **1**, 46-57; c) A. J. Cruz-Cabeza and J. Bernstein, *Chem. Rev*., 2014, **114**, 2170-2191; d) A. Nangia, *Accounts. Chem. Res*., 2008, **41**, 595-604; e) L. Yu, *Accounts. Chem. Res*., 2010, **43**, 1257-1266.

7 K. Wang, H. Zhang, S. Chen, G. Yang, J. Zhang, W. Tian, Z. Su and Y. Wang, *Adv. Mater*., 2014, **26**, 6168-6173.

8 a) Z. G. Chi, X. Q. Zhang, B. J. Xu, X. Zhou, C. P. Ma, Y. Zhang, S. W. Liu and J. R. Xu, *Chem. Soc. Rev*., 2012, **41**, 3878-3896; b) X. Q. Zhang, Z. G. Chi, Y. Zhang, S. W. Liu and J. R. Xu, *J. Mater. Chem. C*, 2013, **1**, 3376-3390.

9 a) W. Z. Yuan, Y. Q. Tan, Y. Y. Gong, P. Lu, J. W. Y. Lam, X. Y. Shen, C. F. Feng, H. H-Y. Sung, Y. W. Lu, I. D. Williams, J. Z. Sun, Y. M. Zhang and B. Z. Tang, *Adv. Mater*., 2013, **25**, 2837-2843; b) H. Li, Z. Chi, B. Xu, X. Zhang, X. Li, S. Liu, Y. Zhang and J. Xu, *J. Mater. Chem*., 2011, **21**, 3760-3767; c) M. P. Aldred, G. F. Zhang, C. Li, G. Chen, T. Chen and M. Q. Zhu, *J. Mater. Chem. C*, 2013, **1**, 6709-6718; d) C. P. Ma, B. J. Xu, G. Y. Xie, J. J. He, X. Zhou,B. Y. Peng, L. Jiang, B. Xu, W. J. Tian, Z. G. Chi, S. W. Liu, Y. Zhang and J. R. Xu, *Chem. Commun*., 2014, **50**, 7374-7377.

10 a) X. Zhang, Z. Chi, J. Zhang, H. Li, B. Xu, X. Li, S.Liu, Y. Zhang and J. Xu, *J. Phys. Chem. B*, 2011, **115**, 7606-7611; b) H. Li, X. Zhang, Z. Chi, B. Xu, W. Zhou, S. Liu, Y. Zhang and J. Xu, *Org. Lett*., 2011, **13**, 556-559; c) Y. J. Dong, J. B. Zhang, X. Tan, L. J. Wang, J. L. Chen, B. Li, L. Ye, B. Xu, B. Zou and W. J. Tian, *J. Mater. Chem. C*, 2013, **1**, 7554-7559.

11 a) J. Kunzelman, M. Kinami, B. R. Crenshaw, J. D. Protasiewicz and C. Weder, *Adv Mater*., 2008, **20**, 119-122; b) S. J. Yoon, J. W. Chung, J. Gierschner, K. S. Kim, M. G. Choi, D. Kim and S. Y. Park, *J. Am. Chem. Soc*., 2010, **132**, 13675-13683; c) J. W. Sun, X. J. Lv, P. J. Wang, Y. J. Zhang, Y. Y. Dai, Q. C. Wu, M. Ouyang and C. Zhang, *J. Mater. Chem. C*, 2014, **2**, 5365-5371.

12 a) G. Zhang, J. Lu, M. Sabat and C. L. Fraser, *J. Am. Chem. Soc*., 2010, **132**, 2160-2162; b) G. Zhang, J. P. Singer, S. E. Kooi, R. E. Evans, E. L. Thomas and C. L. Fraser, *J. Mater. Chem*., 2011, **21**, 8295-8299; c) N. D. Nguyen, G. Zhang, J. Lu, A. E. Sherman and C. L. Fraser, *J. Mater. Chem*., 2011, **21**, 8409-8415; d) G. Zhang, J. Lu and C. L. Fraser, *Inorg. Chem*., 2010, **49**, 10747-10749; e) T. Liu, A. D. Chien, J. Lu, G. Zhang and C. L. Fraser, *J. Mater. Chem*., 2011, **21**, 8401-8408.

13 a) P. Galer, R. C. Korošec, M. Vidmar and B. Šket, *J. Am. Chem. Soc*., 2014, **136**, 7383-7394; b) Q. K. Qi, J. B. Zhang, B. Xu, B. Li, S. X. A. Zhang and W. J. Tian, *J. Phys. Chem. C*, 2013, **117**, 24997-25003; c) S. J. Yoon and S. Y. Park, *J. Mater. Chem*., 2011, **21**, 8338-8346.

14 X. Luo, J. Li, C. Li, L. Heng, Y. Q. Dong, Z. Liu, Z. Bo and B. Z. Tang, *Adv. Mater*., 2011, **23**, 3261-3265.

15 Y. Dong, B. Xu, J. Zhang, X. Tan, L. Wang, J. Chen, H. Lv, S. Wen, B. Li, L. Ye, B. Zou and W. Tian, *Angew. Chem. Int. Ed*., 2012, **51**, 10782-10785.

16 a) Z. Q. Zhang, P. C. Xue, P. Gong, G. H. Zhang, J. Peng and R. Lu, *J. Mater. Chem. C*, 2014, **2**, 9543-9551; b) Z. Q. Zhang, Z. Wu, J. B. Sun, B. Q. Yao, G. H. Zhang, P. C. Xue and R. Lu, *J. Mater. Chem. C*, 2015, **3**, 4921-4932.

17 Y. Zhan, J. Peng, K. Q. Ye, P. C. Xue and R. Lu, *Org. Biomol. Chem*., 2013, **11**, 6814-6823.

18 a) H. P. Zhou, P. C. Xue, Y. Zhang, X. G. Zhao, J. H. Jia, X. F. Zhang, X. L. Liu and R. Lu, *Tetrahedron*, 2011, **67**, 8477-8483; b) J. H. Jia, K. Y. Cao, P. C. Xue, Y. Zhang, H. P. Zhou and R. Lu, *Tetrahedron*, 2012, **68**, 3626-3632; c) J. H. Jia, Y. Zhang, P. C. Xue, P. Zhang, X. Zhao, B. Liu and R. Lu; *Dyes Pigments*, 2013, **96**, 407-413.

19 a) X. Zhao, K. Cao, H. Zhou and R. Lu, *Opt. Mater*., 2014, **36**, 950-957; b) T.-H. Huang, D. Yang, Z.-H. Kang, E.-L. Miao, R. Lu, H.-P. Zhou, F. Wang, G.-W. Wang, P.-F. Cheng, Y.-H. Wang and H.-Z. Zhang, *Opt. Mater*., 2013, **35**, 467-471; c) T.-H. Huang, X.-C. Li, Y.-H. Wang, Z.-H. Kang, R. Lu, E.-L. Miao, F. Wang, G.-W. Wang and H.-Z. Zhang, *Opt. Mater*., 2013, **35**, 1373, 1377.

20 a) X. Liu, X. Zhang, R. Lu, P. Xue, D. Xu and H. Zhou, *J. Mater. Chem*., 2011, **21**, 8756-8765; b) X. Zhang, X. Liu, R. Lu, H. Zhang and P. Gong, *J. Mater. Chem*., 2012, **22**, 1167-1172; c) C. Qian, K. Cao, X. Liu, X. Zhang, D. Xu, P. Xue and R. Lu, *Chinese Sci. Bull*., 2012, **57**, 4264-4271; d) G. Hong, J. Sun, C. Qian, P. Xue, P. Gong, Z. Zhang and R. Lu, *J. Mater. Chem. C*, 2015, **3**, 2371-2379.

21 X. Zhao, P. Xue, K. Wang, P. Chen, P. Zhang and R. Lu, *New J. Chem*., 2014, **38**, 1045-1051.

22 P. Xue, P. Chen, J. Jia, Q. Xu, J. Sun, B. Yao, Z. Zhang and R. Lu, *Chem. Commun*., 2014, **50**, 2569-2571.

23 a) X. Liu, D. Xu, R. Lu, B. Li, C. Qian, P. Xue, X. Zhang and H. Zhou; *Chem. Eur. J*., 2011, **17**, 1660-1669; b) X. Zhang, R. Lu, J. Jia, X. Liu, P. Xue, D. Xu, H. Zhou, *Chem. Commun*., 2010, **46**, 8419-8421; c) C. Qian, M. Liu, G. Hong, P. Xue, P. Gong and R. Lu, *Org. Biomol. Chem*., 2015, **13**, 2986-2998.

24 Rattan Gujadhur, D. Venkataraman and Jeremy T. Kintigh, *Tetrahedron Lett*., 2011, **42**, 4791-4793.

25 J. S. Yang, K. L. Liau, C. M. Wang and C. Y. Hwang, J. Am. Chem. Soc., 2004, 126, 12325-12335.

26 M. J. Frisch, G. W. Trucks, H. B. Schlegel, G. E. Scuseria, M. A. Robb, J. R. Cheeseman, G. Scalmani, V. Barone, B. Mennucci, G. A. Petersson, H. Nakatsuji, M. Caricato, X. Li, H. P. Hratchian, A. F. Izmaylov, J. Bloino, G. Zheng, J. L. Sonnenberg, M. Hada, M. Ehara, K. Toyota, R. Fukuda, J. Hasegawa, M. Ishida, T. Nakajima, Y. Honda, O. Kitao, H. Nakai, T. Vreven, J. A. Montgomery, Jr, J. E. Peralta, F. Ogliaro, M. Bearpark, J. J. Heyd, E. Brothers, K. N. Kudin, V. N. Staroverov, R. Kobayashi, J. Normand, K. Raghavachari, A. Rendell, J. C. Burant, S. S. Iyengar, J. Tomasi, M. Cossi, N. Rega, J. M. Millam, M. Klene, J. E. Knox, J.B. Cross, V. Bakken, C. Adamo, J. Jaramillo, R. Gomperts, R. E. Stratmann, O. Yazyev, A. J. Austin, R. Cammi, C. Pomelli, J. W. Ochterski, R. L. Martin, K. Morokuma, V. G. Zakrzewski, G. A. Voth, P. Salvador, J. J. Dannenberg, S. Dapprich, A. D. Daniels, Ö. Farkas, J. B. Foresman, J. V. Ortiz, J. Cioslowski and D. J. Fox, *Gaussian 09, Revision A.02*, Gaussian, Inc., Wallingford, CT, 2009.

TOC For:

β-Iminoenolate Boron Complex with Terminal Triphenylamine Exhibiting Polymorphism and Mechanofluorochromism

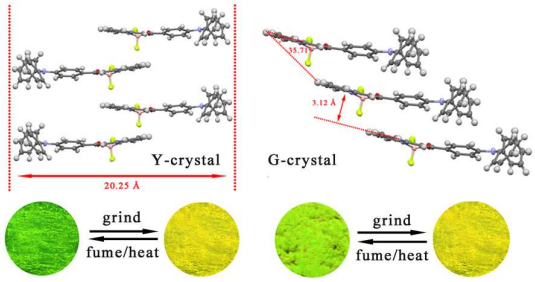

Two kinds of crystals are gained from β-iminoenolate boron complex, and molecular packing mode can be memorized during mechanofluorochromic processes.